doi.org/10.1002/batt.202100134

Nanostructured Carbon Composites from Cigarette Filter Wastes and Graphene Oxide Suitable as Electrodes for 3.4 V Supercapacitors

Juan Luis Gómez-Urbano,[a, b] Gelines Moreno-Fernández,[a] Miguel Granados-Moreno,[a] Teófilo Rojo,[b] and Daniel Carriazo*[a, c]

In this work we report an easy and ecofriendly approach for the preparation of activated carbon-graphene composites using cigarette filter wastes as precursor and evaluate its potential application as electrodes for high energy electrochemical capacitors. Graphene-biowaste derived carbon composites are tested as active electrode materials in three different electrolytes (ammonium salt-based conventional organic electrolyte and two imidazolium-based ionic liquids), which in some of the cases enable to extend the operating voltage windows up to 3.4 V. The incorporation of graphene into the carbon composites not only increase the electronic conductivity but also induce morphological and textural changes that favor the adsorption/desorption of large size ions. Electrical double layer capacitors assembled using these advanced carbon composites can deliver specific capacitances of ca. 160 $F g^{-1}$ at 0.25 $A g^{-1}$ which correspond to energy densities of ca. 65 $Wh kg^{-1}$ at 210 $W kg^{-1}$, when ionic liquids are used as electrolyte. Besides, a comprehensive three-electrode study disclosed that the enhanced capacitance observed for these carbon composites in ionic liquids is related to the optimized textural properties, which improves the imidazolium-cation adsorption.

1. Introduction

In recent times, society is claiming for a sustainable development, pushing international organizations and governments to take actions towards greener and circular economies. Within this context, the demand of renewable energy sources harvested from natural resources such as the sun, wind or sea is growing considerably. Nevertheless, considering their intermittent nature, their fully implementation is directly linked to the development of powerful energy storage systems, that store the excess of energy that is not consumed when is generated.[1] Among the energy storage technologies, electric double layer capacitors (EDLCs), also known as supercapacitors, fill the gap between dielectric capacitors and batteries in terms of power and energy density. The charge is electrostatically stored at the electrode/electrolyte interface by the formation of an electric double layer. Consequently, the charge and discharge can proceed very quickly ensuring high power densities and long cycling stability.[2] However, the lower energy density storage capability of supercapacitors compared to batteries, calls for further research on new electrode active materials and electrolytes. So far, activated carbons (ACs) have been the preferred choice as electrodes in high performing EDLCs due to its large specific surface area and low cost, as well as superior physical and chemical stability.[3] Additionally, ACs can be readily produced from worldwide abundant an easy accessible wastes such as orange peels,[4] rice straw,[5] cherry pits,[6] coffee waste,[7] cigarette butts[8] or paper pulp.[9] The use of wastes as carbon source is not only a simple and cheap approach but also an efficient way to take profit of useless or toxic residues. Among them, cigarette butts (CBs), which is one of the most abundant residues, yearly accounting approximately a million of tons worldwide, are considered an extremely pollutant waste due to its low biodegradability rate and to the presence of highly toxic compounds (heavy metals, polycyclic aromatic hydrocarbons, hydrogen cyanide, etc.) that can be easily released to aquifers and soils.[10] Thus, recycling strategies for CBs wastes should be prioritized.[11] Pyrolysis and activation of acetate cellulose, which is the main component of cigarette filters, for the production of ACs and its application on aqueous-based EDLCs has been previously presented as a promising revalorization strategy.[12–15] However, textural properties of ACs strongly depends on the nature of the precursor used,[16,17] and therefore, they will also have a strong impact on the electrochemical for a certain electrolyte. In this regard, the presence of micropores may increase the specific surface area, but it can also limit the accessibility of the large-sized electrolyte ions, characteristic of organic and ionic liquid electrolytes.[18] On the other hand, the incorporation of nanostructured carbons such as graphene or carbon nanotubes has been found to be useful for increasing the electronic conductivity of the composites and tailoring the particle

[a] J. L. Gómez-Urbano, Dr. G. Moreno-Fernández, M. Granados-Moreno, Dr. D. Carriazo
Centre for Cooperative Research on Alternative Energies (CIC energiGUNE), Basque Research and Technology Alliance (BRTA), 01510 Vitoria-Gasteiz, Spain
E-mail: dcarriazo@cicenergigune.com
[b] J. L. Gómez-Urbano, Prof. T. Rojo
Organic and Inorganic Chemistry Department, University of the Basque Country (UPV/EHU), 48080 Bilbao, Spain
[c] Dr. D. Carriazo
IKERBASQUE, Basque Foundation for Science, 48013 Bilbao, Spain

Supporting information for this article is available on the WWW under https://doi.org/10.1002/batt.202100134

morphology, and their textural properties.[19–21] Besides, electrolyte selection is not a trivial issue since it will mostly determine the operating electrochemical potential window of the cell and thus its energy density. Although more than the 80% of the works published in 2014 used aqueous-based electrolytes,[18] organic electrolytes are still the preferred choice for commercial supercapacitors due to its wider operating potential windows (2.5–2.8 V). However, organic electrolytes, generally formed by conductive salts such as tetraethylammonium tetrafluoroborate (Et_4N BF_4) dissolved in acetonitrile (ACN), still exhibit some volatility, safety and toxicity issues.[22] So, the search for safer and more environmentally friendly electrolytes that can provide larger operating potential windows is one of the priorities of EDLC technology. In the last decade, molten salts at room temperature, generally known as ionic liquids (ILs) have received significant interest as alternative electrolytes for supercapacitors. ILs exhibit several advantages including negligible volatility, non-flammability and good thermal and electrochemical stability (3.0–3.5 V). Nevertheless, the specific capacitance of the final EDLC can be compromise due to the large size of the ILs ions and lower electronic conductivities, so, electrode materials with optimized textural properties are needed.[23,24]

This work focuses on the revalorization of used-cigarette filters as AC source and its application as electrodes for high-voltage EDLCs. Graphene, a bidimensional allotrope of carbon with outstanding conductivity and mechanical properties, is chosen as additive to tailor the morphology and the textural properties of the carbon composites. Its role on the electrochemical performance is investigated using different electrolytes: two imidazolium-based ionic liquids: 1-ethyl-3-methylimidazolium tetrafluoroborate (EMIN BF_4) and 1-ethyl-3-methylimidazolium bis(trifluoromethylsulfonyl)imide (EMIN TFSI), and the conventional organic electrolyte (Et_4NBF_4 in ACN). It is found that the presence of graphene strongly improves the ILs-based supercapacitor performances, especially at high current rates. Specifically, the specific capacitance measured at 10 $A\,g^{-1}$ is boosted from 50 to 130 $F\,g^{-1}$ and from 10 to 120 $F\,g^{-1}$, for EMIN BF_4 and EMIN TFSI, respectively, which together with their wide and stable operating voltage windows allow them to reach outstanding energy densities of ca. 65 $Wh\,kg^{-1}$.

Experimental Section

Activated carbon synthesis

Graphene oxide (Graphenea, 4 $mg\,mL^{-1}$) and cigarette butts, collected from ashtrays, served as carbon precursors. In a first step, remaining tobacco rods, paper and ashes were removed from the cigarette filter and discarded. Then, filters were manually shredded into a fluffy mass of yellow-colored fibers. Cigar waste/GO composite was prepared by mixing 3.0 g of as-obtained fibers and 50 mL of 2 $mg\,mL^{-1}$ graphene oxide. Mixtures were left for 12 h before drying by freeze-freeze drying process to enable the good dispersion of graphene oxide sheets into the filter fibers. Dried precursor composite was pre-carbonized at 400 °C for 3 h using a heating ramp of 5 °C min^{-1} under dynamic Ar atmosphere in a tubular furnace. Then carbon is grounded together with KOH in a mortar using a C:KOH mass ratio of 1:4 and then heated at 800 °C for 1 h under dynamic Ar atmosphere in a tubular furnace using a heating ramp of 5 °C min^{-1}. The resulting material was washed once with a diluted solution of HCl and then several times with hot deionized water. Dry activated carbon, hereafter denoted as GO-FdAC, is obtained after freeze and freeze-drying the material. For the sake of comparison, an activated carbon, denoted as FdAC, was also prepared following the same route but in the absence of graphene oxide.

Physicochemical characterization

Morphological characterization of the samples was performed by scanning electron microscopy (SEM) in a Quanta200 FEI (3 kV, 30 kV) microscope and by transmission electron microscopy (TEM) in a FEI–TECNAI G2 F20 S-TWIN microscope at an acceleration voltage of 200 kV. Raman spectra were recorded with a Renishaw spectrometer (Nanonics Multiview 2000) operating with an excitation wavelength of 532 nm. The spectra were acquired with 30 s of exposition time of the laser beam to the sample. Nitrogen adsorption/desorption isotherms were registered at −196 °C in an ASAP 2460 from Micromeritics. The specific surface area values were calculated using the Brunauer–Emmett–Teller (BET) equation in the relative pressure range between 0.05 and 0.25 and the pore size distributions were calculated by the 2D-NLDFT model applied from the data of the adsorption branches using the SAIEUS software.

Electrochemical characterization

Electrodes of active materials (both GO-FdAC and FdAC) were processed by rolling and pressing a mixture formed by these materials together with Super P C65 and polytetrafluoroethylene in ethanol according to the 90:5:5 mass ratio. Self-standing electrode discs of 11 mm in diameter were punched out from the paste and dried at 120 °C under vacuum overnight prior to cell assembly. AC-based electrodes (4 ± 1 $mg\,cm^{-2}$, 150 ± 30 μm) were evaluated as symmetric EDLCs using a two-electrode Swagelok-type cell. AC-based electrodes were also evaluated in a three-electrode Swagelok-type cell using an oversized Norit (Kuraray) disc as counter electrode and a silver wire as reference electrode (Ag/Ag^+). Whatman D-type glass fiber discs of 13 mm in diameter were used as separator, while 1 M Et_4N BF_4 (Sigma Aldrich, ≥99.0%) in acetonitrile, EMIN BF_4 (Sigma Aldrich, ≥99.0%) and EMIN TFSI (Solvionic, 99.9%) were chosen as electrolytes. Electrochemical impedance spectroscopy (EIS) (signal amplitude 10 mV, frequency range 1 MHz–10 mHz), cyclic voltammetry (CV) and galvanostatic charge-discharge measurements were performed in a multichannel VMP3 generator from Biologic. Operating voltage window for each electrolyte was selected from the cyclic voltammetry measurements following the criteria reported elsewhere.[25] Applied current density (I_g) values were calculated on the basis of the total mass of active material (m_{act}) in the electrodes (90 wt.%). Specific capacitance (C_g) values of the two electrode symmetric cells were calculated from the discharge galvanostatic plots, following Equation (1):

$$C_g = 2 \times \frac{I_g \times t_d}{\Delta V}, \quad (1)$$

where t_d and ΔV are the discharge time and the operational voltage window, respectively, once the total resistance drop is subtracted. Gravimetric energy (E_g) and power densities (P_g) were calculated according to Equations (2) and (3):

$$E_g = \frac{1}{3.6}\left[\frac{1}{8}C_g \times (V_{Max}^2 - V_{Min}^2)\right] \quad (2)$$

$$P_g = \frac{E_g}{t_d}, \quad (3)$$

where V_{Max} and V_{Min} are the maximum and the minimum of the cell potential, once discarded the corresponding resistance drop. Specific capacitance values of the three-electrode cell were calculated from cyclic voltammograms according to Equation (4):

$$C_g = \int \frac{i \times dE}{V_{scan\ rate} \times m_{act}}, \quad (4)$$

where i is the instant current, E is the instant working potential and $V_{Scan\ rate}$ is the applied scan rate in millivolts per second.

2. Results and Discussion

2.1. Physicochemical Characterization

As described in the experimental section, cigarette filters were dispersed within the graphene oxide suspension to maximize the homogeneous distribution of the graphene sheets into the acetate cellulose fibers. Afterwards, the dried composite was submitted to a pre-carbonization step at 400 °C prior the chemical activation. As previously reported, this pre-carbonization step has been proved to be extremely important to enhance the specific surface area of the final ACs,[26] especially when KOH is used as activating agent.[27] SEM images of pre-carbonized samples, with (GO-FdAC precursor) and without graphene (FdAC precursor), are shown in Figure S1. It can be observed that FdAC precursor is formed by large-sized carbon particles (>100 μm) with smooth surface (Figure S1a). The addition of graphene results in a significant reduction of the particle size (<50 μm), which it is also accompanied by a roughening of the carbon surface, and its homogenous coating by graphene sheets (Figure S1b). No significant morphological changes are observed by SEM upon activation of FdAC (Figure 1a). On the contrary, the incorporation of graphene sheets in the GO-FdAC sample (Figure 1b) seems to act as a template during acetate cellulose fibers carbonization. As result, GO-FdAC sample shows a pronounced flat-shaped morphology compared to that of FdAC sample (Figure 1a). TEM image of the GO-FdAC sample clearly shows the uniform growth of acetate cellulose-derived AC on the surface of the graphene sheets (Figure 1c). The Raman spectra (Figure 1d) registered for these materials were deconvoluted to better understand the structural differences between both samples. The fitted spectra show two characteristic D and G bands at ca. 1345 and ca. 1593 cm^{-1}, respectively. From the ratio between band integrated areas (A_D/A_G), values of 2.17 and 1.42 were calculated for FdAC and GO-FdAC, pointing out the lower concentration of defects and a larger degree of graphitization in the graphene containing sample.[28] Additionally, the spectra also show the I and D″ band at ca. 1070 and ca. 1550 cm^{-1}, these bands are related to the disorder in the graphitic lattice and the presence of amorphous phases, respectively. These results agree with the morphological changes induced by the incorporation of the graphene sheets into the carbon composites observed by electron microscopy.

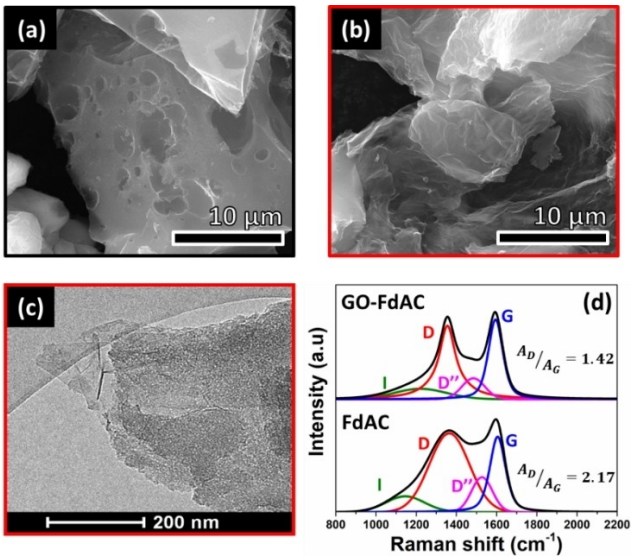

Figure 1. SEM images for FdAC (a) and GO-FdAC (b) activated carbons, TEM image of GO-FdAC (c) and Raman spectra collected and fitted for indicated samples (d).

Textural properties of the activated carbons were determined by nitrogen adsorption/desorption isotherms, which are included in Figure 2(a). According to the IUPAC classification,

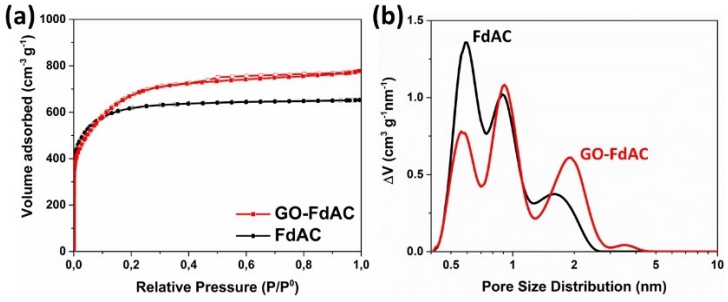

Figure 2. Nitrogen adsorption/desorption isotherms (a) and calculated pore size distributions (b) for GO-FdAC and FdAC samples.

the isotherm of the FdAC sample can be indexed as type I, which corresponds to microporous carbons, while GO-FdAC exhibits a profile in between type-I and IV, characteristic of samples containing a combination of both micropores and mesopores.[29] FdAC and GO-FdAC activated carbons show BET specific surface areas of 2266 and 2252 $m^2 g^{-1}$, respectively. Pore size distributions calculated from the isotherms are depicted in Figure 2(b). Most of the total pore volume of FdAC sample corresponds to the microporous contribution, showing a large amount of small-sized micropores (0.7 nm). On the other hand, the pore size distribution calculated for the GO-FdAC sample is shifted towards larger microporous ranges and small micropores coexist with medium (0.9 nm) and larger ones (2.0 nm). Differences in PSD for both samples can be ascribed to the morphological changes induced by the presence of graphene, as already observed in the SEM images (see Figures 1a and b and S1). Specifically, the graphene sheets act as support for the cellulose acetate fibers, limiting the carbon particle growth and leading to composites with smaller particle size. Under these circumstances the impregnation with KOH is favored leading to the collapse of contiguous micropores into larger size pores.

2.2. Electrochemical Characterization

The performance of the activated carbons was evaluated first in a two-electrode symmetric configuration using one organic electrolyte (1 M Et_4N BF_4 in ACN) and two pure ionic liquids (EMIN BF_4 and EMIN TFSI). The experimental operating voltage window setting for each electrolyte is depicted in Figure S2. As expected, the better electrochemical stability of the imidazolium-based ionic liquids enables a much wider operational window than that of conventional EDLC organic electrolyte. Specifically, operating voltage windows of 2.8, 3.3 and 3.4 V were determined for the Et_4N BF_4, EMIN BF_4 and EMIN TFSI electrolytes, respectively. CVs at different sweep rates included in Figure 3 illustrate the performance of both ACs in those operating voltage ranges. At a first sight, the rectangular-shaped voltammograms reveal the capacitive storage electrostatic mechanism in both of the samples whatever the electrolyte tested. However, the graphene containing sample – GO-FdAC – (Figure 3a–c) outperforms pristine activated carbon – FdAC – (Figure 3d–f) in terms of specific capacitance values and capacitance retention. This fact is much more prominent in the ionic liquid systems. A deeper analysis in the performance of the GO-FdAC in ILs (Figure 3b and c) shows its good capacitance retention, evidenced by the rectangular-shaped profile of CV curves even at very high sweep rates. In contrast, when the graphene-free FdAC sample is tested in ILs, its CV curves get distorted and specific capacity strongly decays when increasing the sweep rates (Figure 3e and f). The good electrochemical performance of GO-FdAC can be ascribed, on one hand to its wider porosity, which enables a fast access of the electrolyte ions to the whole surface of the carbon composite, and, on the other hand, to its better electronic conductivity. On the contrary, the narrow micropores (mainly pores below 0.7 nm) present on the FdAC sample restrict the access of the large $EMIN^+$ and $TFSI^-$ ions with sizes around 0.79 nm (Table 1).

Galvanostatic charge/discharge curves registered at 1 $A g^{-1}$ for the GO-FdAC sample are included in Figure 4(a). In agreement with the CVs measurements, the triangular shape of the charge/discharge curves confirms the electrostatic charge storage mechanism and the absence of faradaic processes on these EDLC systems. It is worth highlighting the negligible ohmic drop observed whatever the electrolyte tested. Just a small voltage decay is observed in the IL-based systems when the current density is increased to 10 $A g^{-1}$ (Figure S3a), which support the outstanding electric conductivity of the graphene-containing sample. In the case of the Et_4NBF_4 electrolyte, no

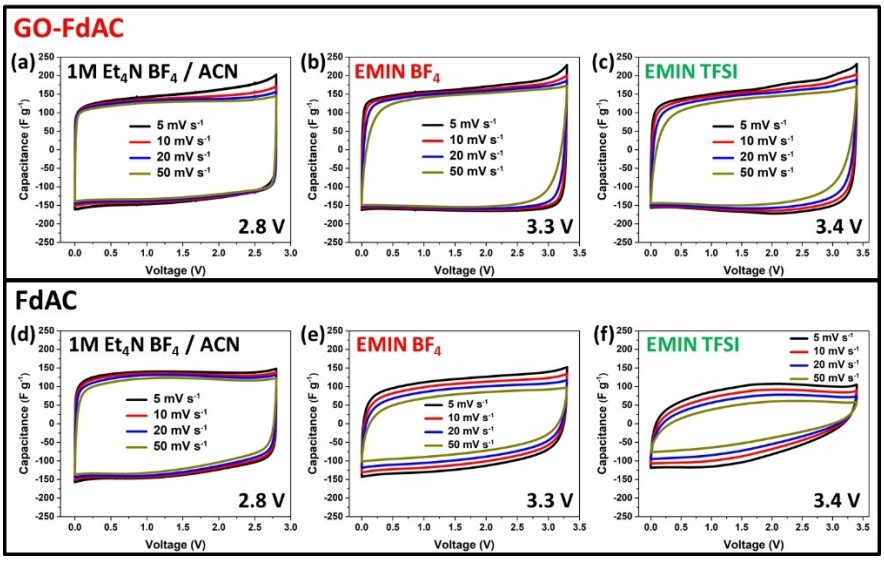

Figure 3. CVs at different scan rates for symmetric EDLCs using GO-FdAC electrodes in Et_4N BF_4 (a), EMIN BF_4 (b) and EMIN TFSI (c), and corresponding measurements for FdAC sample (d–f).

Table 1. Representative physical properties of electrolytes used in this study.

Electrolyte	Viscosity [mPa s]	Conductivity [mS cm^{-1}]	Cation size [nm]	Anion size [nm]	Ref.
1 M Et_4N BF_4 in ACN	0.57	63	0.69	0.46	[30, 31]
EMIN BF_4	37	14	0.76	0.46	[32]
EMIN TFSI	35.55	9	0.76	0.79	[33]

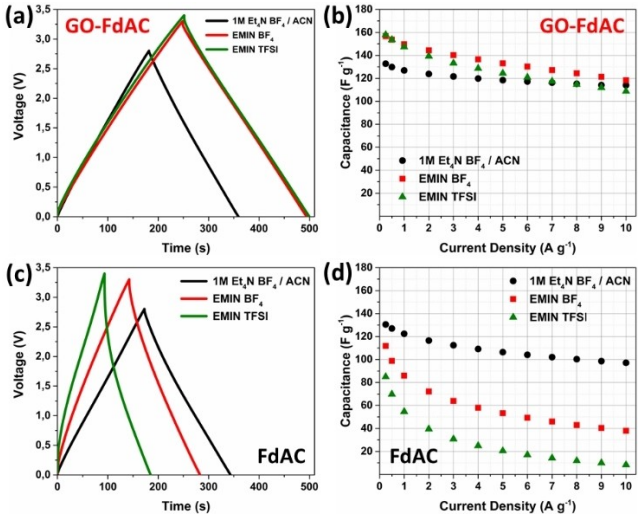

Figure 4. Galvanostatic charge/discharge curves at 1 A g^{-1} (a) and capacitance values at different current densities (b) for GO-FdAC symmetric EDLCs using noted electrolytes and corresponding measurements for FdAC electrodes (c, d).

significant voltage drop is observed whatever the current rate tested. The specific capacitance values for the GO-FdAC sample calculated from the discharge branch of galvanostatic curves at different current rates for all the electrolytes are shown in Figure 4(b). At low current densities (0.25 A g^{-1}), the specific capacitance in ionic liquids is larger than for the conventional organic electrolyte (160 F g^{-1} vs. 132 F g^{-1}). However, Et_4N BF_4 electrolyte shows better capacitance retention at high current densities than ILs (Figure S4a). At 10 A g^{-1}, around 86% of the initial capacitance is retained in the organic electrolyte while 75 and 69% are retained in EMIN BF_4 and EMIN TFSI systems, respectively. This trend is directly related to the viscosity and ionic conductivity values, summarized in Table 1, associated to each of the electrolytes. Conventional organic electrolyte has significant lower viscosity (0.57 mPa s) and higher conductivity (63 mS cm^{-1}) than ILs. And in the case of imidazolium-based electrolytes with similar viscosity (35–37 mPa s), the BF_4^- based salt has higher conductivity compared to the $TFSI^-$ based electrolyte (14 vs. 9 mS cm^{-1} respectively), as reported elsewhere.[30]

Galvanostatic charge/discharge curves registered, and specific capacitance values calculated for the pristine FdAC sample (Figure 4c and d) follow the same electrolyte-dependent trend. However, as also observed in the CVs curves, the graphene-free sample (FdAC) shows a low performance in IL-based electrolytes, which is especially pronounced in the case of the EMIN TFSI. For this system a strong ohmic drop can be observed even at 1 A g^{-1} (Figure 4c), which is accentuated as the current rate is increased (Figure S3b). Specific capacitance values for FdAC sample, depicted in Figure 4(d), strongly decrease as the current density is increased for the IL-based systems. Moreover, at the current density of 10 A g^{-1}, a capacitance retention of just 34% and 10% are measured for the FdAC systems tested in EMIN BF_4 and EMIN TFSI electrolytes, respectively (Figure S4b). In the case of the conventional organic electrolyte (1 M Et_4NBF_4 in ACN) the FdAC sample also shows lower capacitance retention compared with the graphene containing sample (74% vs. 86%, respectively).

So, in an overall aspect, the incorporation of graphene within the carbon composite improves the electrochemical performance of the EDLC systems regardless the electrolyte used. As mentioned above, the presence of the graphene oxide sheets promotes morphological changes during carbonization, which leads to composites with slightly larger micropores that favor the fast adsorption/desorption of large electrolyte ions. Additionally, graphene sheets create a conductive network all along the different AC particles that significantly increases the electric conductivity. Electronic impedance spectroscopy studies, depicted in Figure S5, further confirm the increase of the electronic conductivity and the enhancement of the ionic diffusion for the graphene-containing carbon composite regardless the electrolyte used.

Energy-to-power density plots for the GO-FdAC-based symmetric EDLCs are included in Figure 5(a). The extension of the operating voltage range to 3.3 and 3.4 V leads to outstanding energy densities of 60 and 63 Wh kg^{-1} at 206 and 212 W kg^{-1} for the EMIN BF_4 and EMIN TFSI electrolytes, respectively. At high current densities, EMIN BF_4-based systems overperform the EMIN TFSI-based ones in both energy and power densities due to the better capacitance retention measured in the former electrolyte (41 vs. 37 Wh kg^{-1} at 7,863 and 7,816 W kg^{-1}, respectively). When using the conventional organic electrolyte (Et_4N BF_4 in ACN), the GO-FdAC sample exhibits a slightly lower energy density at low current rates, 36 Wh kg^{-1} at 175 W kg^{-1}, due to its narrower operating voltage window (2.8 V) compared to IL-based systems. But, at high current rates conventional organic-based systems show much better capacitance retention, still delivering 25 Wh kg^{-1} at 26,888 W kg^{-1}. In contrast, Ragone plot for graphene-free activated carbon (FdAC sample, Figure S6a) shows significantly lower energy densities regardless the electrolyte tested.

Stability of the GO-FdAC-based EDLC systems were evaluated through repetitive galvanostatic charge/discharge measurements at 10 A g^{-1} (Figure 5b). It is worth highlighting that in all the cases, graphene-containing system still provides a 78% of the initial capacitance after 11,000 cycles, compared to the 40%–50% of capacitance retention observed for the graphene-free systems (Figure S6b).

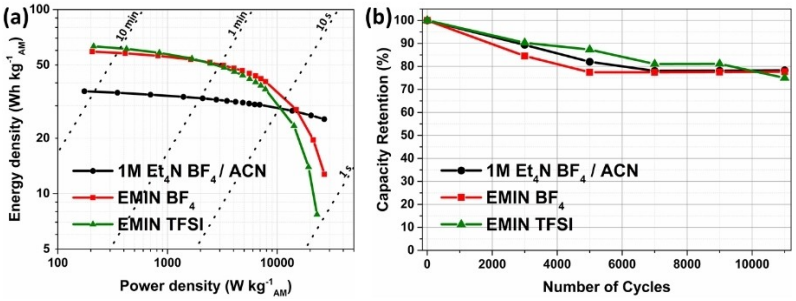

Figure 5. Ragone plots (a) and capacitance retention along galvanostatic cycling at 10 A g^{-1} (b) for GO-FdAC electrodes evaluated as symmetric EDLCs in noted electrolytes.

In Table 2 some representative performance values reported for EDLC systems based on biowaste-derived ACs are summarized. It is worth mentioning, that under these circumstances, EDLC cells assembled using GO-FdAC outperform most of the values reported in literature.

With the objective of improving the rate performance and power density of these EDLCs systems, ACN-diluted ILs solutions were also tested as electrolytes. The GO-FdAC sample evaluated as symmetric EDLCs in diluted ILs show a significant decrease in the resistance compared to those exhibited in pure ILs (Figure S7a). Consequently, they show larger specific capacitance values at faster rates ($>$ 10 A g^{-1}) (Figure S7b), what leads to a better energy and power performance (Figure S8a). However, it is found that the systems based on diluted ILs show a much worse capacitance retention upon cycling (Figure S8b), disabling them for long-term applications. For this reason, they were excluded from the main manuscript (more information about the performance of this carbon composite in diluted ILs is available in the Supporting Information).

In summary, GO-FdAC exhibits very promising electrochemical performance, showing very high energy density and long cycling stability in all the electrolytes tested. So, additionally, in order to get insight on the adsorption processes in each electrode, three-electrode measurements were performed using a silver wire and oversized NORIT discs as reference and counter electrodes respectively. First, the electrochemical stability window of each ion was determined from the open circuit potential (OCP) to its maximum voltage (Figure S9a–c) and subsequently CVs at several scan rates were performed (Figure 6a–c). Figure S9 (a–c) reveals similar stable voltage

Table 2. Summary of the most relevant parameters reported in some recent representative works in EDLC systems using biomass-derived activated carbons in organic and ionic liquid electrolytes.

Material	Surface area [m^2 g^{-1}]	Mass loading [mg cm^{-2}]	Electrolyte	Voltage window [V]	Capacitance [F g^{-1}]	Energy density [Wh kg^{-1}]	Power density [W kg^{-1}]	Cyclability [%]	Ref.
Orange peel derived AC	2160	1.0	EMIN BF$_4$	3.0	140 (0.2 A g^{-1})	43 (300 W kg^{-1})	1,180 (25 Wh kg^{-1})	79% (500 cy)	[4]
Aloe Vera derived AC	1890	2.5	EMIN BF$_4$	3.0	126 (0.1 A g^{-1})	40 (150 W kg^{-1})	800 (15 Wh kg^{-1})	83% (500 cy)	[34]
Rice Straw derived AC	1007	–	EMIN BF$_4$	2.5	80 (0.1 A g^{-1})	17 (126 W kg^{-1})	650 (6 Wh kg^{-1})	78% (5,000 cy)	[5]
Cherry derived AC	1612	3.4	EMIN BF$_4$	3.6	173 (1 A g^{-1})	81 (446 W kg^{-1})	13,650 (25 Wh kg^{-1})	93% (6,000 cy)	[6]
Bamboo derived AC	1472	5.0	EMIN TFSI	3.5	146 (0.2 A g^{-1})	59 (166 W kg^{-1})	42,000 (43 Wh kg^{-1})	95% (5,000 cy)	[35]
Thiourea derived AC	2561	–	EMIN TFSI	3.0	41 (1 A g^{-1})	62 (300 W kg^{-1})	7,560 (26 Wh kg^{-1})	92% (5,000 cy)	[36]
Cellulose derived AC	2285	2.0	EMIN TFSI	3.0	132 (1 A g^{-1})	44 (746 W kg^{-1})	20,000 (18 Wh kg^{-1})	90% (20,000 cy)	[37]
Paper pulp derived AC	2980	2.5	Et$_4$N BF$_4$	2.3	162 (0.1 A g^{-1})	30 (57 W kg^{-1})	5,450 (20 Wh kg^{-1})	–	[9]
			EMIN TFSI	3.0	162 (0.1 A g^{-1})	51 (371 W kg^{-1})	7,000 (31 Wh kg^{-1})	91% (5,000 cy)	
Capsicum derived AC	2201	7.8	EMIN TFSI	3.0	116 (1 A g^{-1})	37 (600 W kg^{-1})	3,000 (25 Wh kg^{-1})	100% (25,000 cy)	[38]
Firmiana derived AC	3320	–	EMIN TFSI	3.0	100 (0.5 A g^{-1})	55 (200 W kg^{-1})	2,083 (42 Wh kg^{-1})	94% (10,000 cy)	[39]
GO-FdAC	2252	4.0	Et$_4$N BF$_4$	2.8	127 (1 A g^{-1})	36 (175 W kg^{-1})	26,880 (25 Wh kg^{-1})	78% (11,000 cy)	This Work
			EMIN BF$_4$	3.3	150 (1 A g^{-1})	60 (206 W kg^{-1})	7,863 (41 Wh kg^{-1})	78% (11,000 cy)	
			EMIN TFSI	3.4	147 (1 A g^{-1})	63 (212 W kg^{-1})	7,816 (37 Wh kg^{-1})	75% (11,000 cy)	

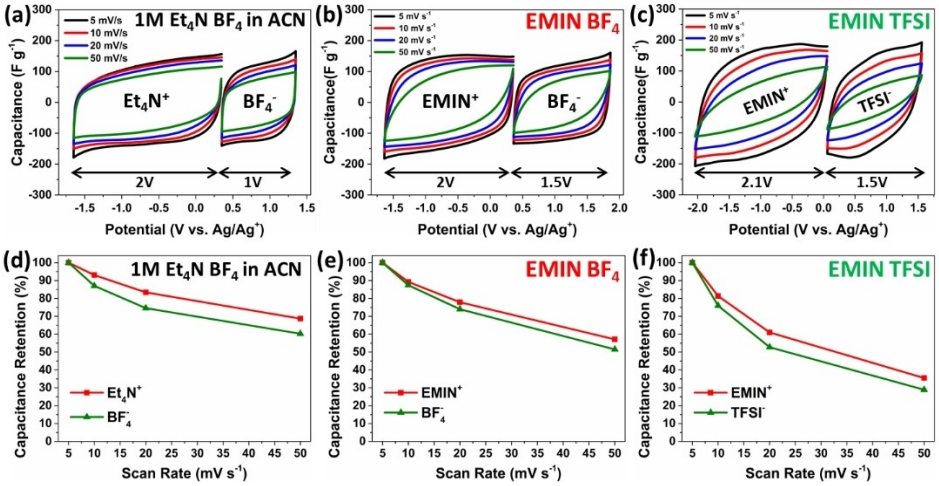

Figure 6. Cyclic voltammetries at different scan rates for Et_4N BF_4 (a), EMIN BF_4 (b) and EMIN TFSI (c) electrolytes, as well as corresponding capacitance retention (d–f) measured for GO-FdAC sample in a three-electrode cell configuration.

windows for the Et_4N^+ and $EMIN^+$ cations. On the other side, the stable voltage window is enlarged for the anions BF_4^- and $TFSI^-$ when taking part of the ILs, which can be the reason for the large operational voltage of both ionic liquids. The higher specific capacitance at lower rates obtained for the ILs in symmetric cells in comparison with the conventional electrolyte (Figures 3 and 4) is related to the higher specific capacitance of the cation $EMIN^+$ compared with that of Et_4N^+ as it is evidenced by three-electrode set up (Figures 6 and S9d–f). Considering that the size of $Et_4N^+ < EMIN^+$ (Table 1) and that most of the total pore volume of GO-FdAC sample arises from pores ~0.9 nm (Figure 2b), the higher capacitance must be related to the different geometry and the better confinement in the pores of $EMIN^+$, as it has been previously reported.[33,40–42] From the comparison of the CV curves at higher rates and the capacitance retention for each ion (Figures 6 and S9), one can conclude that the conductivity of the electrolyte is the main factor limiting the performance at higher rates rather than the viscosity or even the size of the ions.

3. Conclusions

The potential of this ecofriendly and easy-scalable route for the preparation of activated carbons from wasted cigarette filters to be used as electrodes for high voltage EDLCs have been demonstrated. It was found that graphene significantly improves the electrochemical performance of the systems when using ionic liquids and conventional organic electrolytes. The presence of graphene (i) increases the conductivity of the carbon composites, (ii) performs as a template, leading to flat-shaped structures that favors the ions diffusion and (iii) promotes textural modifications, extending the micropores size and thus enabling the adsorption of large-sized electrolyte ions such $EMIN^+$ or $TFSI^-$. Symmetric EDLC supercapacitors assembled using this nanostructured carbon composite as electrode show a specific capacitance value of ca. 160 F g^{-1} at low current rate, and still ca. 120 F g^{-1} at 10 A g^{-1} when tested in ILs. The optimization of this porous carbon composite for their use in imidazolium-based ionic liquids allows delivering energy densities of ca. 63 Wh kg^{-1} at 210 W kg^{-1} and 40 Wh kg^{-1} at 7,800 W kg^{-1} in EMIN BF_4 and EMIN TFSI, respectively. In addition, even when operating at voltage windows above 3.3 V, these systems reach 11,000 charge-discharge cycles with ca. 80% retention of the initial capacitance.

Acknowledgements

The authors thank the Spanish Ministry of Science and Innovation (MICINN/FEDER) [RTI2018-096199-B-I00] for the financial support of this work. J. L. G. U. is very thankful to the Spanish Ministry of Education, Science and Universities (MICINN) for the FPU grant [16/03498]. We are very grateful to María Echeverría for her assistance with TEM measurements. We also want to acknowledge Jean-Luc Dauvergne for providing the cigarette precursors and the company GRAPHENEA for supplying the graphene oxide used in this work.

Conflict of Interest

The authors declare no conflict of interest.

Keywords: biowaste · cigarette · graphene · high voltage · ionic liquid · supercapacitor

[1] M. A. Hannan, M. M. Hoque, A. Mohamed, A. Ayob, *Renewable Sustainable Energy Rev.* **2017**, *69*, 771–789.
[2] P. Simon, Y. Gogotsi, *Nat. Mater.* **2020**, *19*, 1151–1163.
[3] M. Sevilla, R. Mokaya, *Energy Environ. Sci.* **2014**, *7*, 1250–1280.
[4] K. Subramani, N. Sudhan, M. Karnan, M. Sathish, *ChemistrySelect* **2017**, *2*, 11384–11392.

[5] N. Sudhan, K. Subramani, M. Karnan, N. Ilayaraja, M. Sathish, *Energy Fuels* **2017**, *31*, 977–985.
[6] D. Yu, C. Chen, G. Zhao, L. Sun, B. Du, H. Zhang, Z. Li, Y. Sun, F. Besenbacher, M. Yu, *ChemSusChem* **2018**, *11*, 1678–1685.
[7] J. L. Gómez-Urbano, G. Moreno-Fernández, M. Arnaiz, J. Ajuria, T. Rojo, D. Carriazo, *Carbon* **2020**, *162*, 273–282.
[8] T. S. Blankenship, R. Mokaya, *Energy Environ. Sci.* **2017**, *10*, 2552–2562.
[9] H. Wang, Z. Li, K. T. Tak, C. M. B. Holt, X. Tan, Z. Xu, B. S. Amirkhiz, D. Harfield, A. Anyia, T. Stephenson, D. Mitlin, *Carbon* **2013**, *57*, 317–328.
[10] S. Marinello, F. Lolli, R. Gamberini, B. Rimini, *J. Hazard. Mater.* **2020**, *384*, 121245.
[11] J. Torkashvand, M. Farzadkia, *Environ. Sci. Pollut. Res. Int.* **2019**, *26*, 11618–11630.
[12] Q. Meng, W. Chen, L. Wu, J. Lei, X. Liu, W. Zhu, T. Duan, *Energy* **2019**, *189*, 116241.
[13] M. Lee, G.-P. Kim, H. Don Song, S. Park, J. Yi, *Nanotechnology* **2014**, *25*, 345601.
[14] Q. Xiong, Q. Bai, C. Li, D. Li, X. Miao, Y. Shen, H. Uyama, *J. Inst. Chem.* **2019**, *25*, 315–323.
[15] L. Li, C. Jia, X. Zhu, S. Zhang, *J. Cleaner Prod.* **2020**, *256*, 120326.
[16] R. G. Pereira, C. M. Veloso, N. Mendes da Silva, L. Farias de Sousa, R. C. Ferreira Bonomo, A. Oliveira da Souza, M. Oliveira da Guarda Souza, R. da Costa Ilhéu Fontan, *Fuel Process. Technol.* **2014**, *126*, 476–486.
[17] A. R. Tobi, J. O. Dennis, H. M. Zaid, A. A. Adekoya, A. Yar, U. Fahad, *J. Mater. Res. Technol.* **2019**, *8*, 3688–3695.
[18] C. Zhong, Y. Deng, W. Hu, J. Qiao, L. Zhang, J. Zhang, *Chem. Soc. Rev.* **2015**, *44*, 7484–7539.
[19] F. Cheng, X. Yang, S. Zhang, W. Lu, *J. Power Sources* **2020**, *450*, 227678.
[20] G. Moreno-Fernández, J. L. Gómez-Urbano, M. Enterría, T. Rojo, D. Carriazo, *J. Mater. Chem. A* **2019**, *7*, 14646–14655.
[21] G. Moreno-Fernández, M. Granados-Moreno, J. L. Gómez-Urbano, D. Carriazo, *J. Mater. Chem. A* **2021**, *4*, 469–478.
[22] R. Ramachandran, F. Wang, in *Supercapacitors – Theoretical and Practical Solutions*, InTech, **2017**.
[23] L. Yu, G. Z. Chen, *Front. Chem.* **2019**, *7*, 272.
[24] A. Brandt, S. Pohlmann, A. Varzi, A. Balducci, S. Passerini, *MRS Bull.* **2013**, *38*, 554–559.
[25] D. Weingarth, H. Noh, A. Foelske-Schmitz, A. Wokaun, R. Kötz, *Electrochim. Acta* **2013**, *103*, 119–124.
[26] C. H. Yun, Y. H. Park, C. R. Park, *Carbon* **2001**, *39*, 559–567.
[27] M. S. Reza, C. S. Yun, S. Afroze, N. Radenahmad, M. S. A. Bakar, R. Saidur, J. Taweekun, A. K. Azad, *Arab. J. Basic Appl. Sci.* **2020**, *27*, 208–238.
[28] X. Chen, X. Deng, N. Y. Kim, Y. Wang, Y. Huang, L. Peng, M. Huang, X. Zhang, X. Chen, D. Luo, B. Wang, X. Wu, Y. Ma, Z. Lee, R. S. Ruoff, *Carbon* **2018**, *132*, 294–303.
[29] M. Thommes, K. Kaneko, A. V. Neimark, J. P. Olivier, F. Rodriguez-Reinoso, J. Rouquerol, K. S. W. Sing, *Pure Appl. Chem.* **2015**, *87*, 1051–1069.
[30] J. Krummacher, C. Schütter, S. Passerini, A. Balducci, *ChemElectroChem* **2017**, *4*, 353–361.
[31] S. Pohlmann, R.-S. Kühnel, T. A. Centeno, A. Balducci, *ChemElectroChem* **2014**, *1*, 1301–1311.
[32] T. Nishida, Y. Tashiro, M. Yamamoto, *J. Fluorine Chem.* **2003**, *120*, 135–141.
[33] R. Singh, N. N. Rajput, X. He, J. Monk, F. R. Hung, *Phys. Chem. Chem. Phys.* **2013**, *15*, 16090.
[34] M. Karnan, K. Subramani, N. Sudhan, N. Ilayaraja, M. Sathish, *ACS Appl. Mater. Interfaces* **2016**, *8*, 35191–35202.
[35] W. Tian, Q. Gao, Y. Tan, K. Yang, L. Zhu, C. Yang, H. Zhang, *J. Mater. Chem. A* **2015**, *3*, 5656–5664.
[36] L. Ji, B. Wang, Y. Yu, N. Wang, J. Zhao, *Electrochim. Acta* **2020**, *331*, 135348.
[37] Y. Cui, H. Wang, N. Mao, W. Yu, J. Shi, M. Huang, W. Liu, S. Chen, X. Wang, *J. Power Sources* **2017**, *361*, 182–194.
[38] D. Momodu, N. F. Sylla, M. Bridget, A. Bello, T. Masikhwa, S. Lindberg, A. Matic, N. Manyala, *J. Electroanal. Chem.* **2019**, *838*, 119–128.
[39] J. Fang, D. Guo, C. Kang, S. Wan, L. Fu, Q. Liu, *J. Electroanal. Chem.* **2019**, *851*, 113467.
[40] C. Merlet, C. Péan, B. Rotenberg, P. A. Madden, B. Daffos, P.-L. Taberna, P. Simon, M. Salanne, *Nat. Commun.* **2013**, *4*, 2701.
[41] A. Elbourne, S. McDonald, K. Voïchovsky, F. Endres, G. G. Warr, R. Atkin, *ACS Nano* **2015**, *9*, 7608–7620.
[42] G. Moreno-Fernández, N. Boulanger, A. Nordenström, A. Iakunkov, A. Talyzin, D. Carriazo, R. Mysyk, *Electrochim. Acta* **2021**, *370*, 137738.

Manuscript received: June 18, 2021
Revised manuscript received: July 28, 2021
Accepted manuscript online: August 16, 2021
Version of record online: August 28, 2021